Predictive Morphology Control of Hydrogen-Terminated Silicon Nanoparticles

ARTICLE *in* THE JOURNAL OF PHYSICAL CHEMISTRY C · JANUARY 2014

Impact Factor: 4.77 · DOI: 10.1021/jp410652s

2 AUTHORS, INCLUDING:

Amanda S Barnard

The Commonwealth Scientific and Industrial …

181 PUBLICATIONS **4,318** CITATIONS

THE JOURNAL OF PHYSICAL CHEMISTRY C

Article

pubs.acs.org/JPCC

Predictive Morphology Control of Hydrogen-Terminated Silicon Nanoparticles

Hugh F. Wilson* and Amanda S. Barnard

CSIRO Materials Science & Engineering, 343 Royal Parade, Parkville, Victoria, Australia

ABSTRACT: Control of the shape and surface termination of semiconductor nanoparticles via control of the fabrication conditions is desirable for many technological applications. We present a theoretical model based on density functional theory first principles thermodynamics for the optimal shape and surface reconstruction of hydrogen-terminated silicon nanoparticles, as a function of nanoparticle size and the temperature and hydrogen partial pressure of the formation conditions. We predict nanoparticle shapes to be dominated by (111) facets under most conditions, with fully octohedral shapes available for higher H_2 chemical potential and (113) and (001) facets appearing as H_2 chemical potential decreases. Comparison to previously published nanoparticle shapes reveals agreement between the observed and predicted nanoparticle shapes for the reported chemical conditions. Control of the hydrogen chemical potential should allow nanoparticles with variable fractions of (100) and (113) surfaces to be created, with potential applications for functionalization or control of optoelectronic properties.

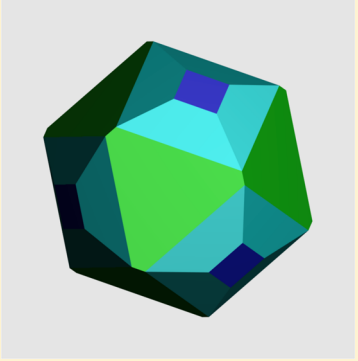

INTRODUCTION

Silicon is a semiconductor of unparalleled technological versatility, and its nanoparticle form has attracted a great deal of interest for a broad variety of applications. Silicon nanoparticles exhibit quantum confinement, making them useful for optoelectronic devices and photocatalysis; however, the optoelectronic properties of a given particle are known to depend in poorly understood ways on the particle size, shape, and surface termination. For medical applications, silicon's apparent nontoxicity[1] and fluorescent properties make it an attractive base for nanoparticle-based diagnostics and therapeutics. Silicon is also attractive as an anode material for lithium ion batteries due to its low discharge potential and extremely high theoretical charge capacity;[2] however, the tendency for silicon to expand dramatically as it absorbs lithium means that anode morphology must be carefully controlled to avoid breakage.[3] For applications in photovoltaics, nanostructured silicon has attractive properties including relatively low cost, low toxicity, and the possibility of multiple exciton generation.[4] For many applications, an increased level of control over nanoparticle shape and the exposure of different surface facets is strongly desirable; shape-engineered nanoparticles may allow detailed control of optical properties (particularly those involving surface plasmon resonances), while selective functionalization of different surfaces may allow catalytic and self-assembling properties of nanoparticles to be exploited.

Silicon nanoparticles may be fabricated via a variety of methods using a number of possible precursor materials, resulting in nanoparticles of various shapes, terminated with a variety of different chemical species.[5] Methods can be divided into solid-state methods which create silicon nanoparticles embedded in a matrix of another solid (e.g SiO_2) and gas- or solid-phase methods which create freestanding nanoparticles, terminated with some chemical species, most commonly hydrogen. Several authors have produced and characterized the morphology of hydrogen-terminated crystalline silicon nanoparticles. Murthy et al. in 1976[6] observed the formation of silicon nanocrystals in thermally decomposed silane/H_2 mixture at 1100 °C. Most (80%) were observed to be octahedral with a smaller portion of tetrahedrons and truncated triangular bipyramids; all these shapes may be composed from (111) surface facets. Körmer et al.[7] used laser-induced pyrolysis of silane to create faceted crystalline silicon nanoparticles whose shapes were detected by high resolution transmission electron microscopy to be very close to octahedral, that is, dominated by (111) facets, but with smaller (100) and (113) facets at the corners. The Kortshagen group[8] has repeatedly used nonthermal silicon−hydrogen plasmas to generate silicon nanoparticles with cubic shapes, and recently the use of nonthermal plasma conditions to create hydrogen-terminated octahedral nanoparticles was also demonstrated.[9] Several methods have also been used for the creation of free-standing silicon nanoparticles terminated with species other than hydrogen, including tetrahedral nanoparticles terminated with chlorine[10] and cubic or octahedral nanoparticles created with a solid−solid Si−SiO_2 interface.[11,12]

Nanoparticle shapes are dependent upon the surface energy and surface stress of the exposed facets of the nanoparticle material as chemically terminated. Although the adsorption of hydrogen on silicon surfaces has been the subject of a large amount of theoretical and experimental work over the years, a complete understanding of silicon surface termination as a function of chemical potential sufficient to allow the prediction

Received: November 13, 2013
Revised: January 5, 2014
Published: January 7, 2014

dx.doi.org/10.1021/jp410652s | J. Phys. Chem. C 2014, 118, 2580−2586

of nanoparticle shapes from formation conditions has not yet been obtained. Hong[13] used density functional theory surface energy calculations to predict equilibrium shapes of hydrogenated silicon crystals but did not include the effect of surface strain or the (113) facet. Barnard and Zapol[14] computed bare and hydrogenated silicon nanocrystal shapes including the effect of surface strain using previously published surface energies but considered only the maximal possible hydrogen coverage rather than conditions of chemical equilibrium, leading to a prediction of cubic nanoparticles valid only in nonequilibrium conditions. In this work we instead construct a predictive model for hydrogen nanoparticle shapes as a function of hydrogen chemical potential across all known surface terminations and validate the model explicitly against experimentally observed nanoparticle shapes. We demonstrate that a range of equilibrium shapes including (111), (113), and (100) surface facets are available for hydrogen-terminated silicon nanoparticles, depending on the chemical potential of gaseous hydrogen. Under conditions of exposure to atomic hydrogen, supersaturation of the surface leads to cubic nanoparticles.

SURFACE ENERGIES

Methodology. Explicit calculation of the energies of nanoparticles of more than a few thousand atoms is both computationally impractical and unnecessary; instead, we may consider the formation energy of a nanoparticle in terms of the energy required to create its surface combined with the energetic influence of the surface upon the bulk. In this work we use a thermodynamic cartography model based on the surface energy and surface stress as used previously in several works.[14−17] The surface energy γ for a bare surface is defined as the energy per unit area required to form a surface from the bulk, generally the energy cost of cleaving bonds minus the energy that can be regained by surface reconstruction. For a surface terminated with an adsorbate, we may include the energy cost of terminating that surface using adsorbate species pulled from a reservoir; the cost of extracting the adsorbate species from its reservoir depends on its chemical potential μ. The energetic cost of forming a nanoparticle of a particular size and shape is thus a sum of contributions from the formation of its surfaces, edges, and corners, with the latter two terms becoming less significant as particle size is increased. Estimates for silicon edge energies are on the order of 1.0×10^{-11} to 5.7×10^{-11} J/m,[14] while surface energies are on the order of 1 J/m^2. Following ref 14, we estimate that the edge and corner energies are of limted significance for nanocrystals larger than 1.6 nm and can be safely neglected for nanoparticles larger than 7.3 nm. The effect of surface stress, which tends to compress the bulk-like portion of the nanoparticle resulting in an additional free energy term that depends on the bulk modulus B_0, is taken into account using a Laplace−Young formalism.[15] Further details on the present model may be found in ref 16.

We begin by computing consistently the surface energies of silicon surfaces as a function of hydrogen coverage. Although all the surface reconstructions under consideration have been studied previously, a set of directly comparable surface energies computed with identical methodologies have not previously been obtained. Four silicon surfaces have been found in theory and experiment to have relatively low surface energies and to be stable against faceting: the (100), (110), (111), and (113) surfaces. The bare and hydrogenated forms of these have been the subject of extensive prior study, with bare and hydrogen-terminated structures proposed for each. Multiple terminations may be observed for each surface depending on exposure; we compute surface energies for each termination previously observed experimentally either for hydrogen or for halogen atoms on each surface.

Calculations in this work were undertaken using the VASP code[18] with pseudopotentials of the projector augmented wave type[19] and the exchange-correlation functional of Perdew, Burke, and Ernzerhof.[20] All calculations used a plane wave basis set with a cutoff of 350 eV. The Brillouin Zone was sampled with a k-point density which was equivalent to 12×12 for the Si(100) 1×1 structure, with the closest possible equivalent density used for other structures. Using these pseudopotentials and parameters, we find an equilibrium bulk lattice constant for silicon of 5.466 Å, which we take to be the underlying lattice constant for all slab calculations. The bulk lattice is found to have a ground state internal energy of −5.424 eV/atom, which we take as the chemical potential for silicon in our calculations.

All systems were simulated in slab geometries terminated identically on each surface, to obtain accurate surface stresses. For Si(100), we used slabs of 18.08 Å thickness (thickness defined as the distance from the top to bottom atom in the bare configuration), for Si(110), slabs of 19.35 Å thickness, for Si(113), slabs of 24.82 Å thickness, and for Si(111), we used slabs of 19.53 Å for the (7×7) reconstruction (consisting of 596 silicon atoms in the bare configuration) and 24.08 Å for the (2×2) reconstruction. A vacuum spacing of at least 12 Å between the extremal silicon atoms of the slab was used in each case.

Surface Energies and Stresses. The Si(100) surface is the most widely studied silicon surface, being the orientation typically used for wafers in semiconductor device manufacture. Cleavage of the Si surface along the (100) direction leaves a uniform grid of 2-fold-coordinated atoms. The atoms reconstruct by joining with a neighbor to form rows of dimers. Each dimer is further stabilized by charge transfer and resulting buckling, which leaves each dimer with an sp^2-like down-atom and an sp^3-like up-atom. Dimers preferentially buckle in the opposite direction to their four surrounding neighbors, making the ground state of the surface a $c(4 \times 2)$ pattern; rapid flipping of the dimers back and forth on microsecond time scales leads to a (2×1) appearance at room temperature, although the presence of surface defects can cause long-range zigzag ordering of dimers.[21] Each silicon dimer retains two dangling bonds which may be satisfied by the addition of two hydrogen atoms. Full termination of all dimers results in a 1 monolayer (ML) coverage.[22] The addition of further adsorbate atoms may be possible possible by the breaking of the Si−Si dimer bonds. Full breakage results in a 2 ML dihydride configuration.[22] The dihydride-saturated dimers show a small energetic preference for canting (tilting) to one side. A (3×1) reconstruction with 4/3 ML coverage of H has also been observed, with alternating rows of 2 ML atoms and 1 ML dimers.[22] Surface energies for the various Si(001) surfaces are shown in Table 1. Notably the 2 ML configuration is chemically unstable compared to the loss of 2/3 of a monolayer to the gas phase for negative values of the chemical potential.

Si(111) has the lowest surface energy of any bare silicon surface. Cleavage of silicon along the Si(111) direction results in an array of 3-fold-coordinated atoms. Although a simpler 2×1 reconstruction, the so-called Pandey chain reconstruction, is frequently formed by low-temperature annealing,[23] the ground state of the bare Si(111) surface is a more complex 7×7

dx.doi.org/10.1021/jp410652s | J. Phys. Chem. C 2014, 118, 2580−2586

Table 1. Surface Energies and Stresses of the Surface Reconstructions and Terminations under Investigation at Zero Temperature and Pressure

surface	termination	γ (J/m^2)	atoms/Å^2	σ (J/m^2)
100	bare	1.25	0	−0.32
	0.5 ML	0.75	0.033	−0.15
	1 ML	0.21	0.067	−0.17
	4/3 ML	0.16	0.089	−0.20
	2 ML	0.26	0.134	+0.17
111	bare (7 × 7)	1.22	0	−2.15
	19/49 ML	0.83	0.030	−2.25
	43/49 ML	0.23	0.067	−1.2
	1 ML	0.07	0.077	+0.02
110	bare	1.49	0	−0.59
	1 ML	0.14	0.092	−0.48
113	bare	1.28	0	−0.59
	1.5 ML (Flege[36])	0.35	0.061	−0.58
	1.5 ML (Hara[35])	0.39	0.061	−1.62

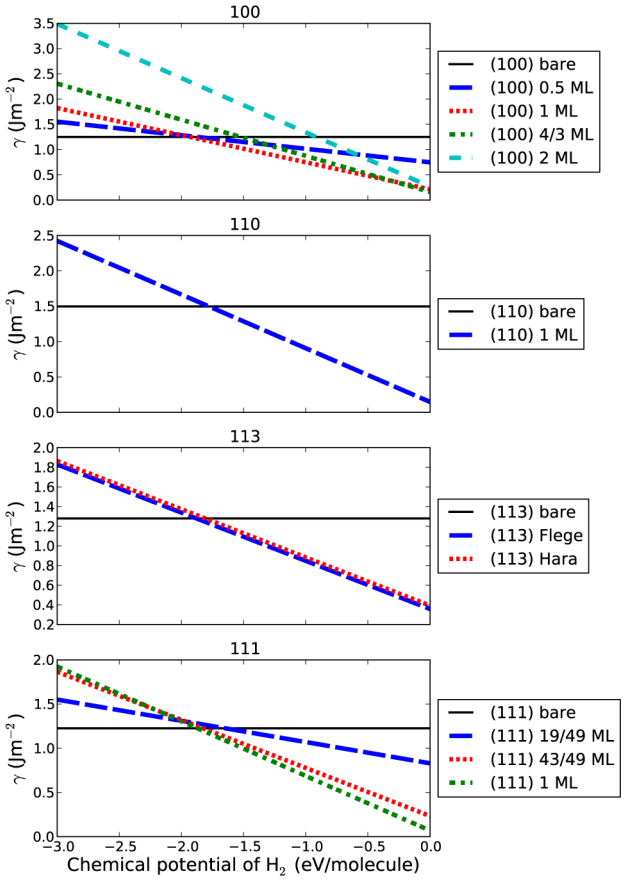

Figure 1. Surface energies of the bare and hydrogen-terminated silicon surfaces as a function of H_2 chemical potential.

reconstruction,[24] known as the dimer-adatom-stacking fault (DAS) surface reconstruction.[25] For hydrogen-like adsorbates on Si(111), three different terminations have been observed. The first is a 7 × 7 19/49 monolayer structure which results from saturating the 19 surface dangling bonds of the DAS (7 × 7) reconstruction.[26] The second is the 7 × 1 structure with 43/49 monolayers, formed by the removal of the ad-dimers from the DAS surface and the saturation of the new dangling bonds thus created. The third is the ideal 1 × 1 reconstruction which results simply from terminating every 3-fold-coordinated atom of the unreconstructed surface with a single adsorbate atom, easily obtained experimentally for hydrogen[27] and halogens.[28] Our calculated surface energies, however, imply a direct transition from the bare to the saturated surface at a μ of approximately −2 eV, without an intermediate range of stability for the 19/49 and 43/49 ML structures at any value of μ.

Although the bare Si(110) surface has the highest surface energy of the surfaces considered here, it may be readily fabricated and has attracted increasing attention in recent years due to hole mobility properties favorable for fin-type transistor manufacture. Cleavage of silicon along the (110) plane results in a (1 × 1) pattern in which each unit cell has two surface atoms, each 3-fold-coordinated, forming zigzag chains running in the [1$\bar{1}$0] direction. Room-temperature reconstruction of the bare surface results in a complex (16 × 2) pattern, whose structure is yet fully understood;[29] however, termination of the surface leads to a simple 1 ML pattern in which each of the 3-fold-coordinated surface atoms acquires one adsorbate atom.[30] As the structure of the (16 × 2) bare surface is not understood, we do not consider it in this work and consider only the (1 × 1) relaxed bare and 1 ML surfaces; because the bare Si(110) surface is far from being competitive with the other bare surface reconstructions, the use of a mildly metastable configuration should not significantly impact our predictions. We predict a transition from the bare to saturated surface at a chemical potential of approximately −1.75 eV.

The Si(113) surface is unique among the high Miller index surfaces of silicon in having a surface energy close to the Si(111) surface, and nonfaceted bare[31] and hydrogenated[32] Si(113) surfaces may be readily prepared. The cleaved Si(113) surface consists of alternating lines of 2-fold coordinated "step" atoms and 3-fold-coordinated "terrace" atoms. Experimentally, the bare Si(113) surface is found to reconstruct with a 3 × 2 symmetry,[33] which may be explained by the adatom-dimer-interstitial (ADI) model of Dabrowski et al.,[34] in which a 6-fold-coordinated subsurface interstitial atom is present. Combined experimental/computational studies have found two possible saturation terminations for Group VII atoms on the Si(113) surface: one by Flege et al. for chlorine and a second by Hara et al.[35] for hydrogen. Although both terminations appear in practice to consist of (2 × n) motifs for several values of n, these appear to be variations on a basic 2 × 2 structure. The Flege et al. structure,[36] which they term a dimer-adatom-on-top (DAO) structure consists of rows of silicon atoms terminated in three different ways: a silicon−silicon dimer, a hydrogen absorbed directly on top of a 3-fold-coordinated silicon, and a silicon adatom bonded to three first-layer silicons and terminated with an on-top terminating atom. The Hara structure is very similar, except that the dimer and on-top part of the motif are instead replaced with a silicon pentamer, which is itself terminated with hydrogen. The results in Table 1 predict that the Flege et al. structure originally proposed for chlorine is slightly more stable than the Hara et al. structure proposed for hydrogen; however, the difference (0.04 J/m^2) is sufficiently small to be within the accuracy of these calculations.

The values we obtain for bare surface energies may be compared to those obtained in previous experimental and theoretical works. In common with the previous LDA work of Stekolnikov[37,38] and Hong[13] as well as the experimental work of Eaglesham based on cavity shapes,[39] we determine the ordering $\gamma(111) < \gamma(100) < \gamma(113) < \gamma(110)$. Similar to the results of three earlier sets of LDA-based calculations, we predict a smaller surface energy difference between the (111)

dx.doi.org/10.1021/jp410652s | J. Phys. Chem. C 2014, 118, 2580−2586

and (100) surfaces, and a larger energy difference between the (111) and (110) surfaces, than is computed in the experimental work of Eaglesham et al.[39] Our predicted surface energies are overall somewhat lower than the LDA-based predictions, consistent with a general tendency for PBE to predict surface energies lower than that for LDA;[40] however, the relative energies of the different surfaces are similar to the LDA-based calculations.

Table 2. Bare Surface Energies at Zero Temperature and Pressure (all in J/m^2) of the Ground-State Bare (100), (110), (111), and (113) Surfaces Determined Experimentally[39] and in Three Different Sets of DFT-LDA Calculations, along with our New DFT-PBE Calculations

surface	this work	expt[39]	LDA[37,38]	LDA[13]	LDA[41]
111	1.22	1.23	1.36	1.45	1.42
100	1.25	1.36	1.41	1.51	1.47
113	1.28	n/a	1.40	n/a	1.52
110	1.49	1.43	1.70	1.99	1.75

The surface stress of each reconstruction must also be known for the nanoparticle model. Although surface stress has little effect on large particles, for small particles with large surface-to-volume ratio, the stress along the surface is sufficient to appreciably compress/stretch the bulk particle. In this work we ignore the anisotropy of the surface strain and compute the surface strain averaged across the two in-plane crystal axes. Strain values for all surfaces and terminations are given in Table 1.

NANOPARTICLE SHAPES

In Figure 2 we plot the formation energies (relative to the bulk silicon and gaseous H_2 phases) of hydrogen-terminated silicon nanoparticles with four simple polyhedral shapes as a function of gas-phase temperature and partial pressure of H_2. The shapes included are the cube, with six (100) faces, the octahedron, with eight (111) faces, the rhombic dodecahedron, with twelve (110) facets, and the deltoidal icosahedron, with twenty-four (113) facets; each shape represents the smallest surface-to-volume ratio for a polyhedron bounded by each particular surface face. The volume of each nanoparticle is equivalent to a sphere of diameter 10 nm. Kinks in each shape's formation energy represent points at which the thermodynamically stable surface termination of the faces changes. For all temperature and pressure conditions, we find that the rhombic dodecahedron (110) shape is uncompetitive. The octahedron (111) is the most stable phase considered across most of the range considered, but the deltoidal icosahedron (113) is more stable for high temperature and low pressure conditions; these are conditions where the chemical potential of hydrogen is low and coverage of the surface is relatively disfavored. For high gas-phase chemical potential, the (111) surface is favored due to the high density of hydrogen bonding sites available in the 1 ML (111) surface.

In general the equilibrium nanoparticle shape is not a simple polyhedron but may have multiple surface facets simultaneously. Optimization of the relative fractions of each surface to minimize the formation energy provides the equilibrium nanoparticle shape. Equilibrium nanoparticle shapes for 10 nm nanoparticles are shown in Figure 3. The gas-phase chemical potential for H_2 is derived from experimental data.[42] High H_2 partial pressure and low temperature result in purely octahedral particle shapes. Raising the temperature or lowering the pressure leads to the formation of (100) and then (113) facets.

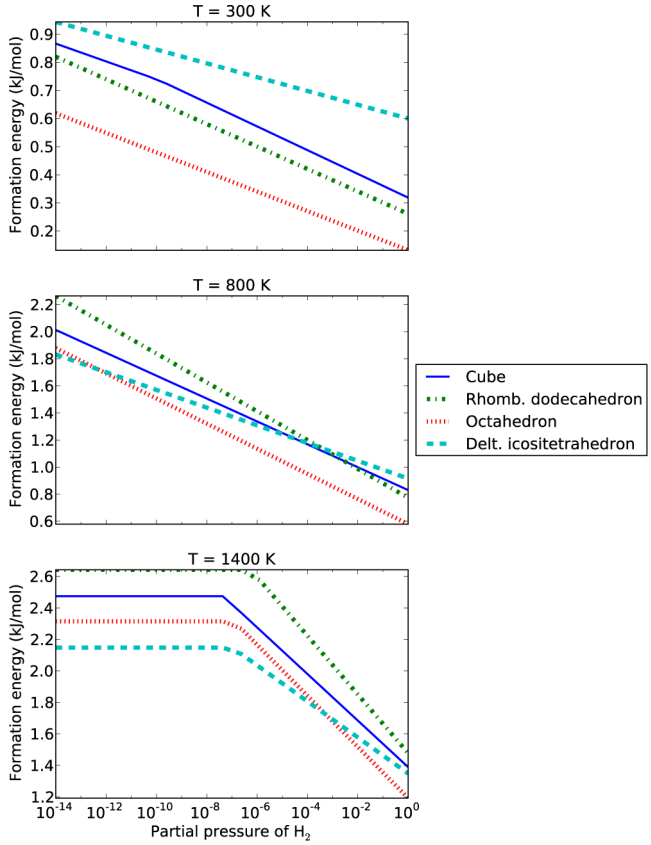

Figure 2. Comparison of simple nanoparticle shapes' formation energies as a function of H_2 pressure and temperature. Included are the cube, with six (100) facets, the octahedron, with eight (111) facets, the rhombic dodecahedron, with twelve (110) facets, and the deltoidal icosahedron, with twenty-four (113) facets. The nanoparticle size in each case is a volume equivalent to a 100 nm diameter sphere.

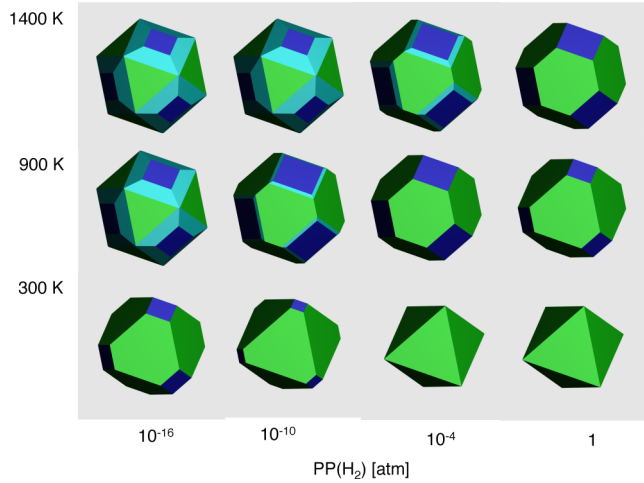

Figure 3. Calculated optimal shape of 10 nm effective diameter silicon nanoparticles as a function of gas-phase temperature and H_2 partial pressure. All nanoparticles have a volume equivalent to a sphere of 10 nm diameter. (111) facets are shown in green, (113) facets in cyan, and (100) facets in dark blue.

dx.doi.org/10.1021/jp410652s | J. Phys. Chem. C 2014, 118, 2580−2586

The variation of predicted nanoparticle shape with respect to nanoparticle size is depicted in Figure 4 for nanoparticles under

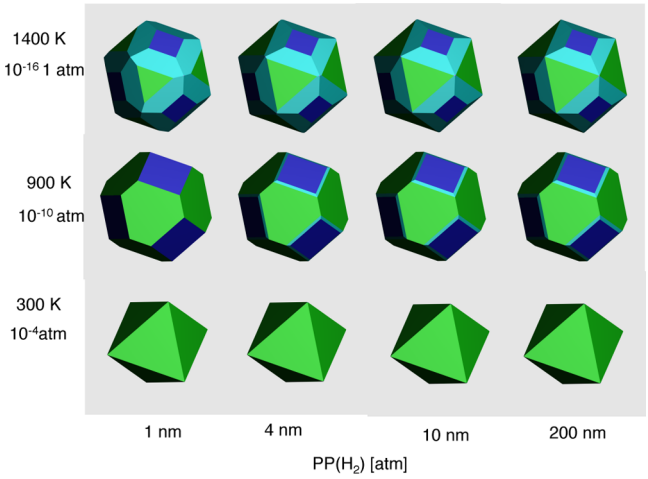

Figure 4. Calculated optimal nanoparticle shape as a function of nanoparticle (volume equivalent spherical) diameter, for three sets of pressure−temperature conditions. (111) facets are shown in green, (113) facets in cyan, and (100) facets in dark blue.

several pressure and temperature conditions. Predicted nanoparticle shapes down to 1 nm are shown, although we expect particles of this size to be beyond the range of applicability of this surface-only model and that explicit calculation of full nanoparticle structure should be more appropriate for nanoparticles in this size regime. Within the applicable size regime of this model, strain effects on morphology appear negligible.

EXPERIMENTAL COMPARISON

The predictions of this model may be compared to previous experimental observations of faceted nanoparticle shapes. The results of Körmer et al.,[7] reproduced in Figure 5, provide transmission electron microscope (TEM) images of nanoparticles grown by thermal pyrolysis of 1 mbar partial pressure silane (in an argon carrier gas) at 1100 °C; this is equivalent to a H_2 partial pressure of 2 mbar. The experimental images clearly show close-to-octahedral silicon nanoparticles but with visible (100) and (113) facets, consistent with our predictions in this pressure regime, although the Körmer nanoparticles appear to be somewhat more (111)-dominated than our predictions at the same conditions, which may be attributable to the neglected effects of edge energies. The older experimental results of Murthy et al.[6] also show near-octahedral nanoparticles, although the resolution of the images is less than that of Körmer et al., making it difficult to identify whether faceting may be present at the corners. The Murthy nanoparticles were formed at an identical temperature (1100 °C) but using hydrogen as a carrier gas, giving a higher partial hydrogen pressure, which our model predicts should increase the dominance of the (111) face over the (113) and (100) faces, compared to the Körmer nanoparticles.

The cubic nanoparticles reported by the Kortshagen group[8] lie outside the scope of this model, due to the nonthermal plasma conditions under which they are formed. Although the temperature of the plasma is not well-defined, we can gain some insight into the shape of these nanoparticles by considering surface energies relative to a reservoir of atomic, rather than molecular, hydrogen. Figure 6 shows the surface

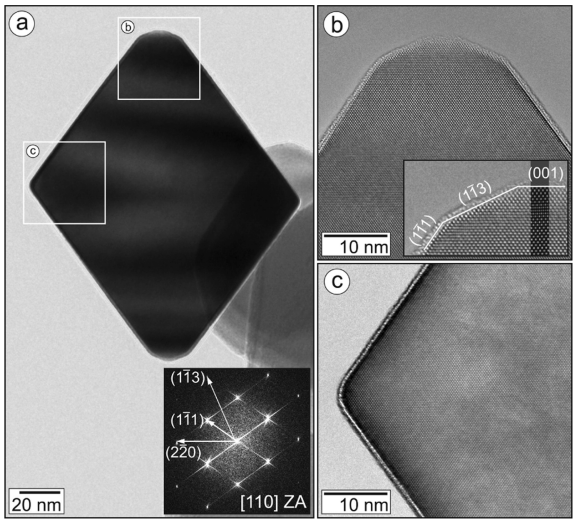

Figure 5. TEM images of nanoparticles formed by pyrolisis of silane at 1100 °C at a partial pressure of 1 mbar in an argon carrier gas. (a) Bright-field TEM image of a single silicon octahedron oriented along the [110] zone axis. (b, c) High-resolution TEM images of the tip as well as along an edge of the octahedron (as indicated in a) revealing the inner crystal structure and faceting. The FFT of such HRTEM image (inset in a) shows the orientation of the lattice with respect to the facets of the SiNP. The main surface facets are (111), with smaller areas of (100) and (113) also exposed. (Reprinted with permission from ref 7. Copyright 2012 American Chemical Society.)

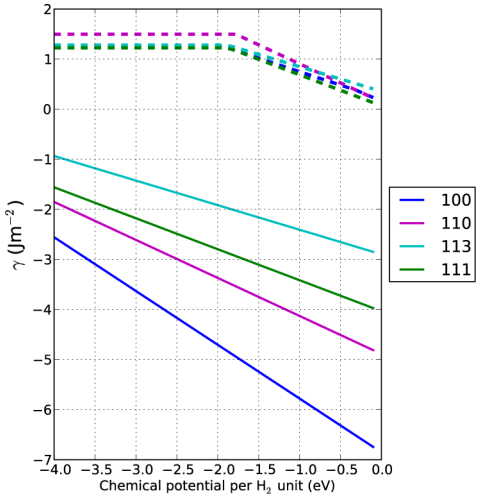

Figure 6. Surface energy of the minimum-energy termination of each Si surface as a function of hydrogen chemical potential relative to a reservoir of molecular H_2 (dotted lines) and atomic hydrogen (solid lines). The surface energies relative to H_2 are similar, but the surface energy of the 2 ML (100) surface is far lower than all other surfaces in the atomic case.

energy of the most stable termination of each surface as a function of hydrogen chemical potential, relative to both a molecular (dotted line) and atomic (solid line) hydrogen reservoir. With the molecular reference state, the energies of different surfaces are relatively close together; however, with the atomic reference state the 2 ML (100), hydrogen termination is significantly more stable than all other configurations studied due to the high density of silicon−hydrogen bonds available on this surface. It is noted experimentally[8] that the cubic nanoparticles formed have

dx.doi.org/10.1021/jp410652s | J. Phys. Chem. C 2014, 118, 2580−2586

SiH_2 and even SiH_3 species on their surface, implying that this supersaturated nonequilibrium surface configuration has been reached under plasma conditions. The recent formation of octahedral nanoparticles in nonthermal plasma conditions by Faraci et al.,[9] and the reason for the difference in shape between the Kortshagen and Faraci nanoparticles, lies likewise beyond the scope of this model.

SUMMARY AND CONCLUSIONS

We have computed the shapes of thermodynamically stable hydrogen-terminated silicon nanoparticles across a broad range of conditions and shown consistency with existing experimental data for nanoparticles formed in a thermal equilibrium system. We have demonstrated that control of pressure and temperature conditions can allow the creation of octahedral nanoparticles or nanoparticles which also include areas of (100) and (113) faceting.

The creation of nanoparticles which present areas of three different surfaces may provide opportunities for selective functionalization of different facets in different ways for the creation of ordered self-assembling nanostructures or the delivery of multiple payloads to the same location in biomedical applications. Understanding of the detailed optopelectronic properties of silicon nanocrystals may allow careful tuning of these properties via surface conditions. Further work to elucidate the behavior of silicon nanoparticle surfaces with differing terminations may be valuable and allow the creation of a broader range of nanoparticle shapes, allowing a wider range of possible applications.

AUTHOR INFORMATION

Corresponding Author

*E-mail: hugh.wilson@csiro.au.

Notes

The authors declare no competing financial interest.

ACKNOWLEDGMENTS

This research was undertaken with the assistance of resources provided at the National Computational Infrastructure systems at the Australian National University. The authors thank Cecilia Noguez for assistance with the Si(111) 7 × 7 geometry, and Haibo Guo for providing relevant code.

REFERENCES

(1) Fujoka, K.; et al. Toxicity Test: Fluorescent Silicon Nanoparticles. *J. Phys.: Conf. Ser.* **2011**, *304*, 012042.

(2) Boukamp, B. A.; Lesh, G. C.; Huggins, R. A. All-Solid Lithium Electrodes with Mixed-Conductor Matrix. *J. Electrochem. Soc.* **1981**, *128*, 725−729.

(3) Liu, X. H.; Zhong, L.; Huang, S.; Mao, S. X.; Zhu, T.; Hyang, J. Y. Size-Dependent Fracture of Silicon Nanoparticles during Lithiation. *ACS Nano* **2012**, *6*, 1522−1531.

(4) Beard, M. C.; Knutsen, K.; Yu, P. R.; Luther, J.; Song, Q.; Metzger, W.; Ellingson, R. J.; Nozik, A. J. Multiple Excition Generation in Colloidal Silicon Nanocrystals. *Nano Lett.* **2007**, *7*, 2506.

(5) Mangolini, L. Synthesis, Properties and Applications of Silicon Nanocrystals. *J. Vac. Sci. Technol., B: Nanotechnol. Microelectron.: Mater., Process., Meas., Phenom.* **2013**, *31*, 020801.

(6) Murthy, T. U. M. S.; Miyamoto, N.; Shimbo, M.; Nishizawa, J. Gas-Phase Nucleation during the Thermal Decomposition of Silane in Hydrogen. *J. Cryst. Growth* **1976**, *33*, 1.

(7) Körmer, R.; Butz, B.; Spiecker, E.; Peukert, W. Crystal Shape Engineering of Silicon Nanoparticles in a Thermal Aerosol Reactor. *Cryst. Growth. Des.* **2012**, *12*, 1330−1336.

(8) Uwe Kortshagen, L. M.; Bapat, A. Plasma Synthesis of Semiconductor Nanocrystals for Nanoelectronics and Luminescence Applications. *J. Nanopart. Res.* **2006**, *2007*, 39−52.

(9) Faraci, G.; Pennisi, A. R.; Alberti, A.; Ruggeri, R.; Mannino, G. Giant Photoluminescence Emission in Crystalline Faceted Si Grains. *Sci. Rep.* **2013**, *3*, 2674.

(10) Baldwin, R. K.; Pettigrew, K. A.; Garno, J. C.; Power, P. P.; Liu, G.-y.; Kauzlarich, S. M. Room Temperature Solution Synthesis of Alkyl-Capped Tetrahedral Shaped Silicon Nanoparticles. *J. Am. Chem. Soc.* **2002**, *124*, 1150−1151.

(11) Yang, Z.; Dobbie, A. R.; Cui, K.; Veinot, J. G. C. A Convenient Method for Preparing Alkyl-Functionalized Silicon Nanocubes. *J. Am. Chem. Soc.* **2012**, *134*, 13958−13961.

(12) Hessel, C. M.; Henderson, E. J.; Veinot, J. G. C. Hydrogen Silsesquioxane: A Molecular Precursor for Nanocrystalline $Si-SiO_2$ Composites and Freestanding Hydride-Surface-Terminated Silicon Nanoparticles. *Chem. Mater.* **2006**, *18*, 6139−6146.

(13) Hong, S. Equilibrium Shape of Hydrogen-Covered Diamond and Silicon Surfaces. *J. Kor. Phys. Soc.* **2000**, *37*, 93−98.

(14) Barnard, A. S.; Zapol, P. A Model for the Phase Stability of Arbitrary Nanoparticles as a Function of Size and Shape. *J. Chem. Phys.* **2004**, *121*, 4276−4283.

(15) Barnard, A. S. A Thermodynamic Model for the Shape and Stability of Twinned Nanostructures. *J. Phys. Chem. B* **2006**, *110*, 24498.

(16) Barnard, A. S. Modelling of Nanoparticles: Approaches to Morphology and Evolution. *Rep. Prog. Phys.* **2010**, *73*, 086502.

(17) Guo, H.; Barnard, A. S. Thermodynamic Modelling of Nanomorphologies of Hematite and Goethite. *J. Mater. Chem.* **2011**, *21*, 11566.

(18) Kresse, G.; Furthmüller, J. Efficient Iterative Schemes for *Ab Initio* Total-Energy Calculations Using a Plane-Wave Basis Set. *Phys. Rev. B* **1996**, *54*, 11169−11186.

(19) Blöchl, P. E. Projector Augmented Wave Method. *Phys. Rev. B* **1994**, *50*, 17953−17979.

(20) Perdew, J. P.; Burke, K.; Ernzerhof, M. Generalized Gradient Approximation Made Simple. *Phys. Rev. Lett.* **1996**, *77*, 3865−3868.

(21) Wilson, H. F.; Marks, N. A.; McKenzie, D. R. Defect-Induced Dimer Pinning on the Si(001) Surface. *Surf. Sci.* **2005**, *587*, 185−192.

(22) Boland, J. J. Structure of the H-Saturated Si(100) Surface. *Phys. Rev. Lett.* **1990**, *65*, 3325−3328.

(23) Pandey, K. C. New π-Bonded Chain Model for Si(111)-(2 × 1) Surface. *Phys. Rev. Lett.* **1981**, *47*, 1913−1917.

(24) Takayanagi, K.; Tanishiro, Y.; Takahashi, S.; Takahashi, M. Structure Analysis of Si(111)-7 × 7 Reconstructed Surface by Transmission Electron Diffraction. *Surf. Sci.* **1985**, *164*, 367−392.

(25) Brommer, K. D.; Needels, M.; Larson, B.; Joannopoulos, J. D. Ab-Initio Theory of the Si(111)-(7 × 7) Surface Reconstruction: A Challenge for Massively Parallel Computation. *Phys. Rev. Lett.* **1992**, *68*, 1355−1358.

(26) Noguez, C.; Beitia, C.; Preyss, W.; Shkrebtii, A. I.; Roy, M.; Borensztein, Y.; Sole, R. D. Theoretical and Experimental Optical Spectroscopy Study of Hydrogen Adsorption at Si(111)-(7 × 7). *Phys. Rev. Lett.* **1996**, *76*, 4923−4926.

(27) Higashi, G. S.; Chabal, Y. J.; Trucks, G. W.; Raghavachari, K. Ideal Hydrogen Termination of the Si(111) Surface. *Appl. Phys. Lett.* **1990**, *56*, 656−658.

(28) Eves, B. J.; Lopinski, G. P. Formation and Reactivity of High Quality Halogen Terminated Si(111) Surfaces. *Surf. Sci.* **2005**, *579*, 89−96.

(29) Setvín, M.; Brázdová, V.; Bowler, D. R.; Tomatsu, K.; Nakatsuji, K.; Komori, F.; Miki, K. Electronic Structure of Si(110)-(16 × 2) Studied by Scanning Tunneling Spectroscopy and Density Functional Theory. *Phys. Rev. B* **2011**, *84*, 115317.

(30) Arima, K.; Katoh, J.; Endo, K. Atomic-Scale Analysis of Hydrogen-Terminated Si(110) Surfaces After Wet Cleaning. *Appl. Phys. Lett.* **2004**, *85*, 6254−6256.

(31) Gibson, J. M.; McDonald, M. L.; Underwald, F. C. Direct Imaging of a Novel Silicon Surface Reconstruction. *Phys. Rev. Lett.* **1985**, *55*, 1765−1767.
(32) Jacobi, K.; Gruyters, M.; Geng, P.; Bitzer, T.; Aggour, M.; Rauscher, S.; Lewerenz, H.-J. Hydrogenation of Si(113) Surfaces by Photoelectrochemical Treatment. *Phys. Rev. B* **1995**, *51*, 5437−5440.
(33) Myler, U.; Jacobi, K. On the Electronic and Geometric Structure of the Si(113) Surface. *Surf. Sci.* **1989**, *220*, 353−367.
(34) Dąbrowski, J.; Müssig, H.-J.; Wolff, G. Atomic Structure of Clean Si(113) Surface: Theory and Experiment. *Phys. Rev. Lett.* **1994**, *73*, 1660−1663.
(35) Hara, S.; Suzuki, T.; Takahashi, I.; Ohsumi, T.; Fuse, K.; Fujishiro, H. I.; Irokawa, K.; Miki, H.; Kawazu, A. Study of H:Si(113) 2 × 2 Structure by Scanning Tunneling Microscopy and *Ab Initio* Calculation. *e-J. Surf. Sci. Nanotechnol.* **2010**, *8*, 261−265.
(36) Flege, J. I.; Schmidt, T.; Siebert, M.; Materlik, G.; Falta, J. Atomic Structure of Chlorinated Si(113) Surfaces. *Phys. Rev. B* **2008**, *78*, 085317.
(37) Stekolnikov, A. A.; Furthmüller, J.; Bechstedt, F. Absolute Surface Energies of Group-IV Semiconductors: Dependence on Orientation and Reconstruction. *Phys. Rev. B* **2002**, *65*, 115318.
(38) Stekolnikov, A. A.; Furthmüller, J.; Bechstedt, F. Adatoms, Dimers, and Interstitials on Group-IV(113) Surfaces: First-Principles Studies of Energetical, Structural and Electronic Properties. *Phys. Rev. B* **2003**, *67*, 195332.
(39) Eaglesham, D. J.; White, A. E.; Feldman, L. C.; Moriya, N.; Jacobson, D. C. Equilibrium Shape of Si. *Phys. Rev. Lett.* **1993**, *70*, 1643−1646.
(40) Hsing, C.-R.; Wei, C.-M. Quantum Monte Carlo Study of Surface Energy. In *APS March Meeting Abstracts*; APS March Meeting 2012, Boston, MA, Feb 27−Mar 2, 2012; p A5012.
(41) Lu, G. H.; Huang, M.; Cuma, M.; Liu, F. Relative Stability of Si Surfaces: A First-Principles Study. *Surf. Sci.* **2005**, *588*, 61−70.
(42) Chase, M. W.; Davis, C. A.; Downey, J. R.; Frurip, D. J.; McDonald, R. A.; Syverud, A. N. JANAF Thermochemical Tables, 3rd ed. *J. Phys. Chem. Ref. Data* **1985**, *14*.